Article

Not peer-reviewed version

Heterocyclic Derivatives Bearing 4-Pyridyl Substituents; Multitarget Biological Evaluation

Monika Pitucha *, Paweł Szymański, Mateusz Jędrzejec, Anna Gajda, Bartłomiej Rogalewicz, Ewelina Fornal, Anita Raducka, Marcin Świątkowski, Magdalena Iwan, Agnieszka Korga-Plewko, Edyta Kordialik-Bogacka, Sylwia Ścieszka, Marek Smoluch, Agnieszka Czylkowska *

Posted Date: 2 April 2026

doi: 10.20944/preprints202604.0146.v1

Keywords: thiosemicarbazone; anticancer; antioxidant; antibacterial; ADME analysis

 doi:10.20944/preprints202604.0146.v1

Article

Heterocyclic Derivatives Bearing 4-Pyridyl Substituents; Multitarget Biological Evaluation

Monika Pitucha [1,*], Paweł Szymański [2,3], Mateusz Jędrzejec [3], Anna Gajda [4], Bartłomiej Rogalewicz [5], Ewelina Fornal [5], Anita Raducka [5], Marcin Świątkowski [5], Magdalena Iwan [6], Agnieszka Korga-Plewko [7], Edyta Kordialik-Bogacka [8], Sylwia Ścieszka [8], Marek Smoluch [9] and Agnieszka Czylkowska [5,*]

[1] Independent Radiopharmacy Unit, Faculty of Pharmacy, Medical University of Lublin, Chodźki 4a, 20-093 Lublin, Poland
[2] Department of Medical Biology, Military Institute of Hygiene and Epidemiology, Kozielska 4, 01-163 Warsaw, Poland
[3] Department of Pharmaceutical Chemistry, Drug Analyses and Radiopharmacy, Faculty of Pharmacy, Medical University of Lodz, Muszyńskiego 1, 90-151 Łódź, Poland
[4] Institute of Organic Chemistry, Faculty of Chemistry, Lodz University of Technology, Żeromskiego 114, 90-924 Łódź, Poland
[5] Institute of General and Ecological Chemistry, Faculty of Chemistry, Lodz University of Technology, Żeromskiego 114, 90-543 Łódź, Poland
[6] Department of Toxicology, Medical University of Lublin, Chodźki 8b, 20-093 Lublin, Poland
[7] Independent Medical Biology Unit, Medical University of Lublin, Jaczewskiego 8b, 20-093 Lublin, Poland
[8] Institute of Fermentation Technology and Microbiology, Faculty of Biotechnology and Food Sciences, Lodz University of Technology, Wólczańska 171/173, 90-924 Łódź, Poland
[9] Faculty of Materials Science and Ceramics, AGH University, Mickiewicza 30, 30-059 Kraków, Poland
* Correspondence: monika.pitucha@umlub.edu.pl (M.P.); agnieszka.czylkowska@p.lodz.pl (A.C.)

Abstract

This study focuses on the multitarget biological evaluation of variously substituted 4-pyridyl thiosemicarbazones. Six compounds (**C1**-**C6**) containing chlorine atoms in different positions of the phenyl ring were synthesized, and their structures were confirmed using mass spectrometry, FTIR, and NMR spectroscopy. Biological evaluation included antioxidant activity assays (ABTS, DPPH, and ORAC-FL), antibacterial testing against Gram-positive and Gram-negative bacteria, and anticancer activity assessment against a panel of cancer cell lines (A375, G-361, LNCaP, Caco-2, and U-87 MG), as well as healthy fibroblasts (BJ) to evaluate selectivity. While the compounds exhibited limited antibacterial activity, more pronounced anticancer effects were observed, particularly for a singly chlorinated derivative, with reduced cytotoxicity toward healthy cells. No direct correlation was observed between anticancer and antioxidant activities. Finally, ADME analysis suggested favorable pharmacokinetic profiles for all six compounds.

Keywords: thiosemicarbazone; anticancer; antioxidant; antibacterial; ADME analysis

1. Introduction

While studied for decades, thiosemicarbazones remain a valuable class of compounds due to their diverse biological activities and their versatility as synthetic intermediates, particularly as precursors for the preparation of five- and six-membered heterocyclic systems such as thiazolidinones, thiazolines, pyrazoles, and 1,2,4-triazoles [1]. Due to their interesting properties, thiosemicarbazones and their derivatives continue to receive ever-growing attention [2]. These compounds exhibit a wide spectrum of biological properties, including antibacterial activity, especially against Gram-positive and Gram-negative bacteria [3–5], as well as anticancer activity,

 doi:10.20944/preprints202604.0146.v1

acting on various types of cancers, such as leukemia [6,7], pancreatic [8], breast [9,10], non-small cell lung [11], cervical [12,13], prostate [14,15], and skin cancers [16]. Simultaneously, according to predictions of the International Agency for Research on Cancer, the total number of new cancer cases will increase from 20.0 million in 2022 to 32.6 million in 2045 [17]. Additionally, around 1.27 million deaths were directly caused by antibiotic-resistant bacterial infections in 2019, with antibiotic resistance contributing to a total of 4.95 million deaths worldwide [18]. These statistics highlight the urgent need to develop new, safer, and more efficient drugs.

Thiosemicarbazone scaffold is present in several compounds with high therapeutic potential, some of which have entered clinical trials, especially for cancer treatment (Figure 1). The N,N,S donor system seems to be crucial for anticancer activity of thiosemicarbazones, enabling several distinct modes of action, including intracellular iron and copper chelation, inhibition of key enzymes like topoisomerases and ribonucleotide reductase (RNR), and generation of reactive oxygen species (ROS) [19]. Although sharing the same thiosemicarbazone core, their mechanisms of action, bioavailability, and systemic toxicity are significantly different. For example, while the action of 3-AP mainly involves inhibition of RNR, COTI-2 relies on reactivation of mutant p53 to its wild-type form [7,20]. Among those presented, DpC appears to exhibit the fewest side effects [21]. Interestingly, while the anticancer activity of thiosemicarbazones is strongly modulated by complexation with metal ions, our previous results suggest that their antibacterial activity is often more strain-specific, yielding comparable results for organic ligands and their metal complexes [3,22]. Another example of a compound containing the thiosemicarbazone backbone is metisazone, a well-known antiviral drug.

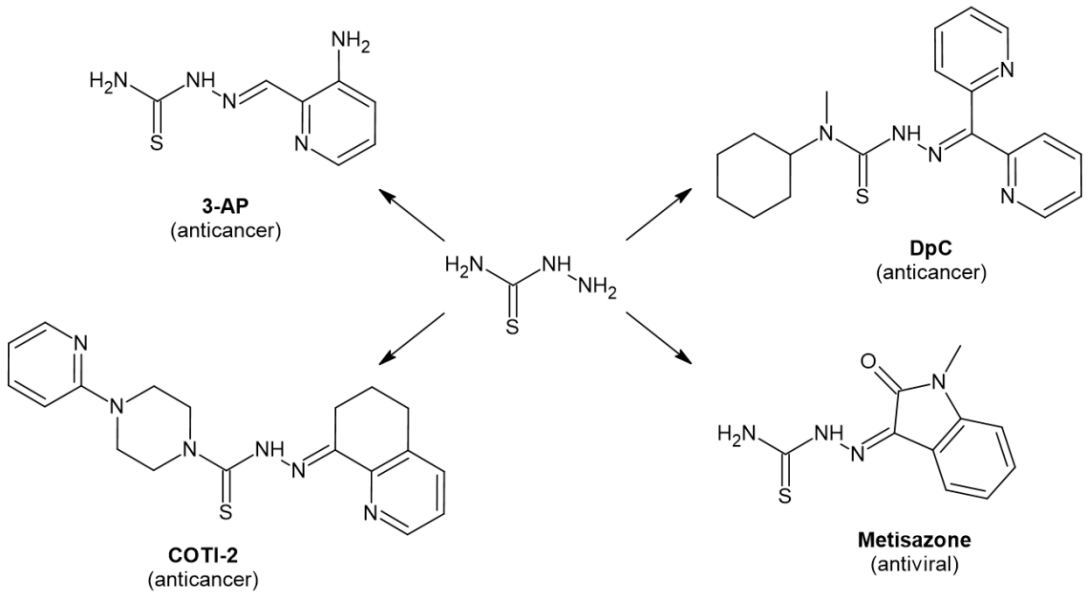

Figure 1. Thiosemicarbazide and some of its bioactive derivatives.

In contemporary drug discovery, multitarget evaluation has emerged as an important strategy to address complex diseases by simultaneously modulating multiple biological pathways with a single molecular entity. Both pyridine and thiosemicarbazone moieties are well-recognized pharmacophoric fragments: pyridine rings frequently enhance target binding, solubility, and metabolic stability, while thiosemicarbazones provide versatile metal-chelating and enzyme-interacting functionalities responsible for a broad spectrum of biological activities. The combination of these fragments within a single molecular framework enables the rational design of molecular hybrids with enhanced and complementary biological effects.

One of the most important characteristics of the thiosemicarbazone scaffold is its tunability. Depending on the introduced substituents and moieties, the physicochemical properties, pharmacokinetic profile, and biological activity of the resulting compound can be fine-tuned. At the same time, the chlorine substituent is a simple yet important modification that appears to play a

 doi:10.20944/preprints202604.0146.v1

special role in drug discovery [23,24]. Studies have shown that the substitution with chlorine atoms can increase the anticancer activity of fluoren-9-one derivatives compared to analogs without the chlorine atom [25]. The introduction of chlorine atoms into molecules can also affect the antibacterial and antifungal activity of compounds [26–28]. The nature of the substituents on the aryl ring determines both the spectrum and intensity of the inhibitory effect against microorganisms [25]. Chlorine atoms in the structure of aripiprazole, an antipsychotic drug, control the geometry and movement of the molecule at the binding site with human serum albumin, which translates into its unique pharmacological properties compared to the derivative without chlorine atoms [29]. In summary, numerous studies confirm that the introduction of chlorine atoms into the molecules of biologically active compounds can significantly modify their activity by changing interactions with receptors and other molecular targets. This effect is widely used in the design of drugs with the desired pharmacological profile [30–32].

This study aims to comprehensively investigate biological activities, pharmacokinetic profiles, and physicochemical properties of six 4-pyridyl-based thiosemicarbazones variously substituted with chlorine atoms. It represents a continuation of our previous research, in which we studied analogous compounds, but bearing 2-pyridyl moiety [33].

2. Results and Discussion

2.1. Synthesis and Structural Characterization

The title compounds (**C1**-**C6**) were prepared by reacting 4-pyridinecarboxaldehyde with the appropriate thiosemicarbazides: 4-phenyl-3-thiosemicarbazide, 4-(2-chlorophenyl)-3-thiosemicarbazide, 4-(3-chlorophenyl)-3-thiosemicarbazide, 4-(4-chlorophenyl)-3-thiosemicarbazide, 4-(2,4-dichlorophenyl)-3-thiosemicarbazide, 4-(2,6-dichlorophenyl)-3-thiosemicarbazide (Scheme 1).

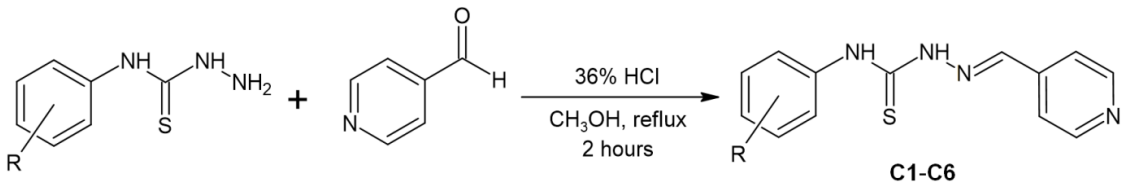

R	Compound
H	**C1**
2-Cl	**C2**
3-Cl	**C3**
4-Cl	**C4**
2,4-diCl	**C5**
2,6-diCl	**C6**

Scheme 1. Synthesis of compounds **C1**-**C6**.

Later, the compounds were analyzed utilizing the appropriate analytical techniques, including ^{1}H and ^{13}C NMR spectroscopy (Figures S1-S12), HRMS (Figures S13-S18, Table S1), and FTIR spectroscopy (Figures S19-S24). The synthesized compounds exhibit spectral features typical for thiosemicarbazones. In the ^{1}H NMR spectra of the obtained compounds, characteristic singlets corresponding to the protons of the functional groups were observed: NH–C=S in the range of 12.00-12.30 ppm, NH–N=CH in the range of 10.20-10.30 ppm, and C(H)=N at 8.09-8.13 ppm. Furthermore, signals of the pyridine ring protons are visible in two regions: 7.83-7.88 ppm and 8.60-8.64 ppm, as well as differentiated signals of the phenyl ring protons occurring in the range of 7.20-7.74 ppm, the exact shape and position of which depend on the type of substitution. The ^{13}C NMR spectra of the studied thiosemicarbazones show a characteristic signal of the C=S/C=N carbon atom in the range of 176-178 ppm, C-2/C-6 signals of the pyridine ring at approximately 150 ppm, and signals of the remaining pyridine atoms in the range of 140-142 ppm. In the range of 126-138 ppm, a set of signals originating from the phenyl ring is observed, the exact position of which depends on the type and

 doi:10.20944/preprints202604.0146.v1

number of chloro substituents. In the HRMS spectra, the expected $[M+H]^+$ ions were observed in all cases, showing good agreement between the calculated and experimental values (Table S1). Additionally, the FTIR spectra display several distinctive bands corresponding to different vibrational modes. Sharp bands observed in the 3350-3250 cm^{-1} region are attributed to ν(NH) stretching vibrations. Less intensive bands appearing below 2900 cm^{-1} are assigned to ν(CH) modes. Similarly, bands characteristic for aromatic ν(CC) stretching vibrations are observed below 1600 cm^{-1}, followed by bands tentatively assigned to ν(CN), δ(CH), and δ(NH) modes.

Single-Crystal X-Ray Diffraction

The molecular structure of compound **C6** was determined using single-crystal X-ray diffraction. The compound crystallizes as a monosolvate with DMSO (Figure 2a). The structural analysis reveals characteristic features typical for thiosemicarbazones (Table 1). The C7-S1 bond length corresponds to the thione form commonly observed in thioureas [1.681(20) Å], while the C8-N3 bond distance is consistent with an imine bond character [1.279(8) Å] [35]. The C1-N1-C7-N2-N3-C8-C9 chain adopts a trans-cis-trans-trans conformation, which is stabilized by intramolecular N1—H1•••N3 hydrogen bonding forming an S(5) motif (Table 2). In addition to this intramolecular interaction, the amino group N1 participates in a bifurcated hydrogen bonding system, with the pyridine ring nitrogen N4 serving as the second acceptor. This specific hydrogen bonding with the pyridine nitrogen generates a C(10) chain synthon that directly organizes the molecules into a right-handed helical arrangement (Figure 2b), which is responsible for the crystallization in the chiral $P2_12_12_1$ space group. The DMSO solvent molecule is stabilized within the crystal lattice through intermolecular N2—H2•••O21 hydrogen bonding with a finite D(2) motif. The geometry of **C6** molecule shows significant non-planarity, with the dihedral angle between the mean planes of the benzene and pyridine rings measuring 73.2°. Due to this pronounced angular orientation, the crystal packing reveals an absence of π-π stacking interactions between the aromatic rings.

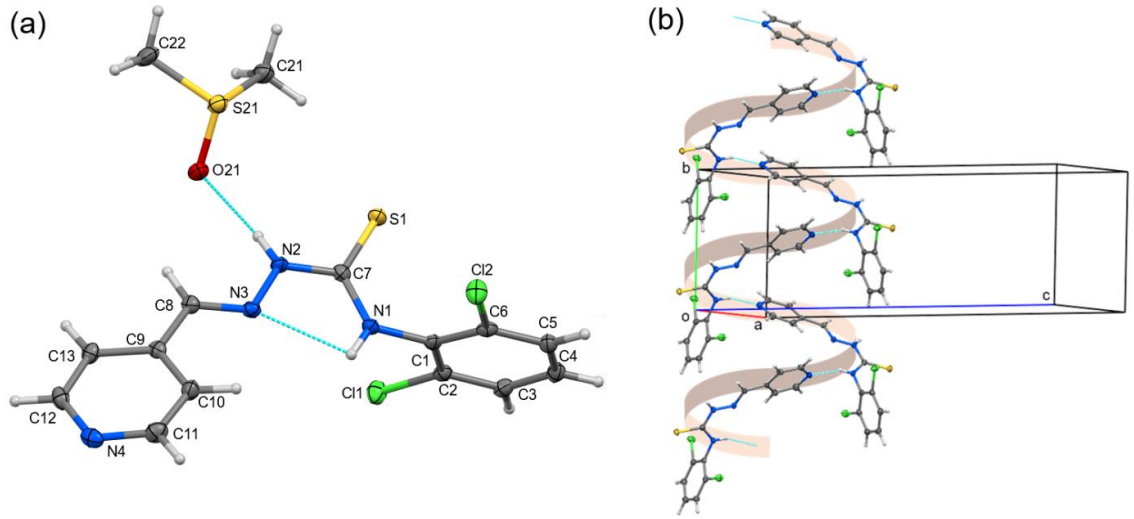

Figure 2. Molecular structure of **C6** (plotted with 50% probability of displacement ellipsoids) with highlighted S(6) and D(2) hydrogen bonds (a); Hydrogen bond right-handed helix motif in the structure of **C6** propagated via C(10) synthon (b).

Table 1. Selected structural data (d – bond length, α – angle, τ – torsion angle) of **C6**.

i—j	d_{ij} (Å)	i—j—k	α_{ijk} (°)	i—j—k—l	τ_{ijkl} (°)
C1—N1	1.416(3)	C1—N1—C7	120.5(2)	C1—N1—C7—N2	173.7(2)
N1—C7	1.338(3)	N1—C7—S1	124.02(19)	N1—C7—N2—N3	2.8(3)
C7—S1	1.682(3)	N1—C7—N2	116.6(2)	C7—N2—N3—C8	-169.7(2)

 doi:10.20944/preprints202604.0146.v1

C7—N2	1.359(3)	S1—C7—N2	119.40(19)	N2—N3—C8—C9	-178.6(2)
N2—N3	1.371(3)	C7—N2—N3	119.2(2)		
N3—C8	1.282(3)	N2—N3—C8	115.9(2)		
C8—C9	1.470(3)	N3—C8—C9	119.1(2)		

Table 2. Hydrogen bonds in **C6** [d – distance, < – angle, $G_d^a(n)$ – unitary graph set].

D-H•••A	d(D—H) (Å)	d(H•••A) (Å)	d(D•••A) (Å)	<(DHA) (°)	$G_d^a(n)$
N1—H1•••N3	0.82(3)	2.31(3)	2.627(3)	104(3)	S(5)
N1—H1•••N4[i]	0.82(3)	2.08(3)	2.848(3)	157(3)	C(10)
N2—H2•••O21	0.85(3)	1.94(3)	2.776(3)	169(3)	D(2)

Symmetry transformations used to generate equivalent atoms: [i] -x, 1/2+y, 1/2-z.

2.2. Antioxidant Activity

Antioxidant properties constitute fundamental physicochemical characteristics of numerous biologically active compounds [34–37]. It has been shown that antioxidants can significantly reduce cancer incidence and progression, and that elevated levels of reactive oxygen species (ROS) can result in gene mutations and disruption of cell signaling, thereby contributing to carcinogenesis. Although numerous therapeutic strategies are currently in use or under clinical investigation, their effectiveness and safety often remain unsatisfactory. For this reason, the search for new drugs among compounds with strong antioxidant properties represents a promising approach. Therapeutic strategies to modulate oxidative stress include direct ROS scavengers (e.g., vitamins, N-acetylcysteine, GSH derivatives), indirect antioxidant regulators such as NRF2 activators that enhance cellular defense systems, and agents targeting enzymatic ROS metabolism or production (e.g., NOX inhibitors and SOD mimics) [38,39].

The antioxidant capacity of the tested thiosemicarbazones was evaluated using ABTS, DPPH, and ORAC-FL assays, with Trolox used as the reference standard (Table 3). In the ABTS assay, compound **C6** exhibited antioxidant activity comparable to Trolox, while compounds **C1** and **C3** showed similar IC_{50} values, and compounds **C2**, **C4** and **C5** displayed weaker radical scavenging activity. In the DPPH assay, all tested compounds demonstrated lower antioxidant activity than Trolox, although compounds **C1**, **C2**, **C3**, and **C5** retained measurable radical scavenging capacity. Evaluation of **C6** was not possible due to insufficient absorbance data. The ORAC-FL assay revealed antioxidant activity for all compounds, with **C6** showing the highest Trolox-equivalent value, whereas **C1** exhibited the lowest activity. Compounds **C2**-**C4** showed comparable ORAC-FL values. Overall, while the results indicate assay-dependent differences in antioxidant performance among the tested compounds, **C6** consistently demonstrated the strongest activity across the applied methods. Most of the compounds studied here exhibited equal or slightly improved antioxidant capacity in the DPPH and ORAC-FL assays compared with previously reported analogous compounds containing a 2-pyridyl moiety [33]. Overall, both series displayed comparable levels of antioxidant activity.

Table 3. ABTS, DPPH and ORAC-FL results for assessing the total antioxidant capacity.

Compound	IC_{50} ± SD (mg/mL)		TC* ± SD (μM/g)
	ABTS	DPPH	ORAC-FL
C1	0.020 ± 0.001	0.043 ± 0.002	0.035 ± 0.001
C2	0.035 ± 0.006	0.030 ± 0.001	0.022 ± 0.001
C3	0.021 ± 0.003	0.036 ± 0.008	0.028 ± 0.001
C4	0.046 ± 0.002	0.077 ± 0.007	0.022 ± 0.001

 doi:10.20944/preprints202604.0146.v1

C5	0.170 ± 0.060	0.043 ± 0.000	0.031 ± 0.001
C6	0.016 ± 0.001	-	0.016 ± 0.001
Trolox (STD)	0.015 ± 0.002	0.013 ± 0.002	1.000 ± 0.000

2.3. Anticancer Activity

To evaluate the anticancer potential of the title thiosemicarbazones, their activity was assessed against five human cancer cell lines, including malignant melanomas (A375, G-361), prostate cancer (LNCaP), colorectal adenocarcinoma (Caco-2), and malignant glioma (U-87 MG). For comparison, cytotoxicity toward healthy human fibroblasts (BJ) was also examined. The obtained IC_{50} values are presented in Table 4, while the corresponding dose-response curves showing cell viability are provided in the Supplementary Materials (Figures S25-S30). While most compounds did not induce significant growth inhibition, compound **C2** emerged as the most versatile derivative, exhibiting pronounced activity against LNCaP cells and moderate activity against A375, G-361, and U-87 MG cell lines. Importantly, in all cases, the viability of normal BJ fibroblasts remained above 80% even at the highest tested concentration (100 μM). Notably, **C2** was among the least toxic compounds toward normal fibroblasts, with 90.26% cell viability observed at 100 μM, indicating a favorable selectivity profile.

Table 4. Anticancer activity of the tested thiosemicarbazones.

Compound	IC_{50} ± SD [μM]					
	A375	G-361	LNCaP	Caco-2	U-87 MG	BJ
C1	>100	>100	60.25 ± 0.52	>100	>100	>100
C2	76.80 ± 7.62	81.66 ± 2.36	53.85 ± 0.83	>100	97.28 ± 2.79	>100
C3	>100	>100	>100	>100	>100	>100
C4	>100	>100	>100	>100	>100	>100
C5	>100	>100	>100	>100	>100	>100
C6	>100	>100	>100	>100	>100	>100

2.4. Antibacterial Activity

Most bacterial strains were not sensitive to the tested substances, and the minimum inhibitory concentration (MIC) values were mainly >1000 mg/L, except for compound **C1** against *Listeria monocytogenes* ATCC 19115, and **C3** against *Staphylococcus aureus* ATCC 25923. The most promising results were obtained for the *Bacillus cereus* strain, for which MIC values ranged from 50 to 1000 mg/L (Table 3). The activity was markedly lower than that of the reference antibiotics, ciprofloxacin and vancomycin, and, in most cases, also lower in comparison with similar derivatives investigated by us. In this previous study, thiosemicarbazones containing a 2-pyridyl moiety exhibited a moderate activity against Gram-positive strains, particularly *B. cereus* and *S. aureus*, with MIC values ranging from 10 to >1000 mg/L, depending on the compound [33]. Notably, compounds lacking a chlorine substituent (**C1**) or containing a single chlorine atom (**C2**-**C4**) were more active than the dichlorinated derivatives (**C5**, **C6**), in agreement with our previous findings [33].

Table 3. Minimum inhibitory concentration (MIC) values of the investigated compounds against the tested microorganisms.

	MIC [mg/L]						
	C1	**C2**	**C3**	**C4**	**C5**	**C6**	Reference

 doi:10.20944/preprints202604.0146.v1

							(Van/Cip)*
Gram-negative bacteria							
Escherichia coli ATCC 10530	>1000	>1000	>1000	>1000	>1000	>1000	1
Salmonella Typhimurium ATCC 14028	>1000	>1000	>1000	>1000	>1000	>1000	1
Gram-positive bacteria							
Bacillus cereus ŁOCK 0807	1000	50	1000	50	>1000	>1000	1
Bacillus subtilis ATCC 6633	>1000	>1000	>1000	>1000	>1000	>1000	1
Enterococcus faecalis ATCC 29212	>1000	>1000	>1000	>1000	>1000	>1000	2
Staphylococcus aureus ATCC 25923	>1000	>1000	1000	>1000	>1000	>1000	1
Staphylococcus aureus ATCC 6538	>1000	>1000	>1000	>1000	>1000	>1000	1
Staphylococcus epidermidis ATCC 12228	>1000	>1000	>1000	>1000	>1000	>1000	1
Listeria monocytogenes ATCC 19115	1000	>1000	>1000	>1000	>1000	>1000	2

*Vancomycin and ciprofloxacin were used as reference positive controls for Gram-positive bacteria and Gram-negative bacteria, respectively.

2.4. ADME Analysis

The ADME analysis results (Figure 3, Table 4) for the six analyzed compounds (**C1**-**C6**) show that all compounds exhibit moderate water solubility, with Log S values ranging from -4.36 to -5.45. This may suggest the possibility of oral administration, but may also require additional formulation techniques to improve solubility. According to the BOILED-Egg diagram (Figure 4), all compounds are characterized by high absorption in the gastrointestinal tract, indicating good bioavailability after oral administration. Additionally, none of them penetrates the blood-brain barrier, which may limit their use in the treatment of central nervous system disorders, but may be beneficial when targeting peripheral tissues. While all compounds are predicted to be inhibitors of CYP1A2, CYP2C19, CYP2C9, suggesting potential drug interactions, none of them is predicted to be a glycoprotein P substrate. The compounds meet the criteria of Lipinski [40], Ghose [41], Veber [42], Egan [43], and Muegge [44], indicating their potential as drug candidates. Overall, the pharmacokinetic profiles of the investigated thiosemicarbazones are similar to those obtained for the recently studied analogous compounds based on a 2-pyridyl moiety [33]. While the physicochemical characteristics may be comparable, the different position of the nitrogen atom in the aromatic ring is expected to more strongly influence metal-ion chelation and enzyme binding affinities, thereby influencing activity at the mechanistic level.

Table 4. Basic pharmacokinetic properties of the studied ligands. Log S is calculated as an average of three different predictions: ESOL, Ali, SILICOS-IT. Log P is calculated as an average of five different predictions: iLOGP, XLOGP3, WLOGP, MLOGP, and SILICOS-IT.

	Molecular weight [g/mol]	TPSA [Å²]	Log S	Log P	CYP1A2 inhibitor	CYP2C19 inhibitor	CYP2C9 inhibitor	CYP2D6 inhibitor	CYP3A4 inhibitor
C1	256.33	81.40	-4.83	2.58	Yes	Yes	Yes	No	No
C2	290.77	81.40	-4.36	2.73	Yes	Yes	Yes	No	No
C3	290.77	81.40	-5.45	3.12	Yes	Yes	Yes	No	Yes

 doi:10.20944/preprints202604.0146.v1

C4	290.77	81.40	-5.45	3.13	Yes	Yes	Yes	No	Yes
C5	325.22	81.40	-4.97	3.27	Yes	Yes	Yes	No	Yes
C6	325.22	81.40	-4.97	3.25	Yes	Yes	Yes	No	Yes

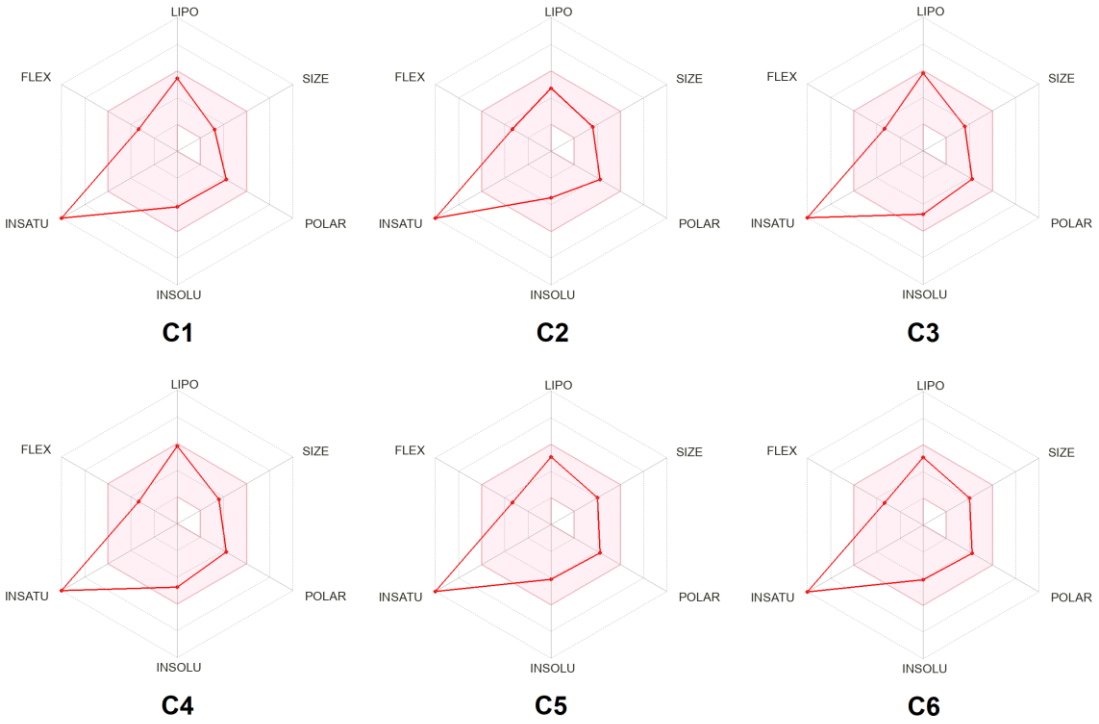

Figure 3. Bioavailability radars generated using the SwissADME service. The red-colored zone is considered physicochemically suitable for oral bioavailability. LIPO – lipophility (-0.7 < XlogP3 < 5.0); SIZE – molecular weight (150 g/mol < MW < 500 g/mol); POLAR – polarity (20 Å^2 < TPSA <130 Å^2); INSOLU – insolubility (-6 < logS < 0); INSATU – insaturation (0.25 < fraction Csp3 < 1); FLEX – flexibility (0 < num. of rotatable bonds < 9).

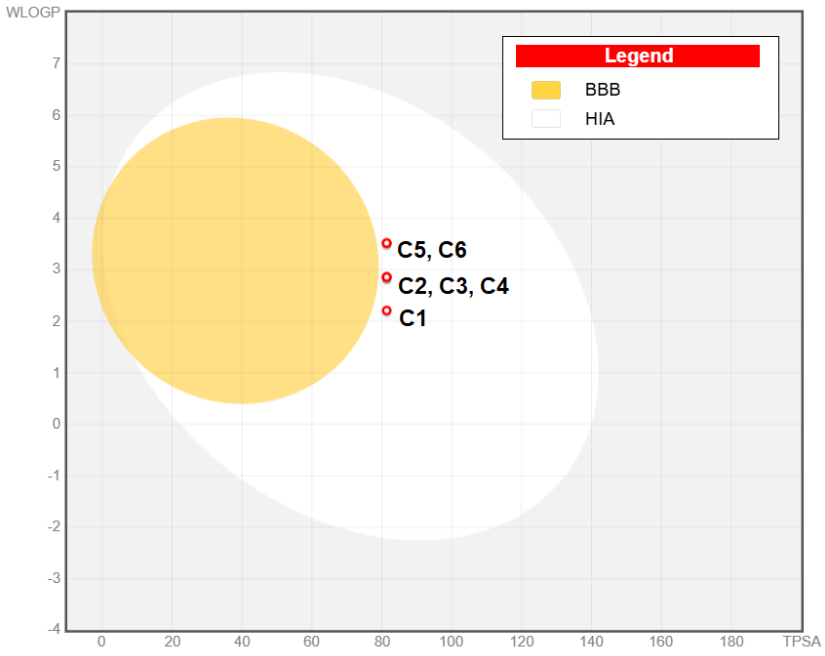

Figure 4. The BOILED-Egg diagram obtained for **C1**-**C6**. The white area represents high gastrointestinal absorption; the yellow area represents the blood-brain barrier permeation.

 doi:10.20944/preprints202604.0146.v1

2.5. Molecular Docking

Since the observed anticancer activity does not correlate strongly with the antioxidant activity, molecular docking was performed to evaluate the possible enzyme inhibition of **C1**-**C6**. The molecular targets were closely related to the studied cancer cell lines and involved B-Raf Kinase V600E (BRAF), human Androgen Receptor (hAR), Epidermal Growth Factor Receptor (EGFR), and Lipid Kinase PI3K alpha (PI3K). BRAF V600E is a hallmark mutation in many malignant melanomas [45]. At the same time, the Androgen Receptor (hAR) represents one of the most important molecular targets in prostate cancer therapy [46]. Additionally, the Epidermal Growth Factor Receptor (EGFR) is frequently overexpressed in glioblastoma, including the U-87 MG cell line, where it plays a key role in promoting cell proliferation and survival [47]. Furthermore, Phosphoinositide 3-kinase (PI3K) is a central component of the PI3K/AKT signaling pathway, which is commonly dysregulated in cancer and is associated with enhanced tumor growth, survival, and resistance to therapy [48].

The obtained results showed partial correlation with the observed anticancer activity. Overall, the docking scores for compounds **C1**-**C6** were comparable (Table 5). Interestingly, although the most active compounds (**C1** and **C2**) exhibited effective binding to some targets (BRAF, hAR), the highest docking scores were observed for **C3** (BRAF), **C6** (hAR), and **C5** (EGFR, PI3K). The ligand-target complexes with the highest docking scores were visualized in both 2D (Figures 5 and 6) and 3D (Figures S31-S34). In the case of the **C3**-BRAF and **C5**-PI3K, the ligand-protein complexes were stabilized primarily by hydrophobic interactions. In contrast, additional hydrogen bonds were identified for the **C6**-hAR and **C5**-EGFR complexes. For the **C6**-hAR complex, hydrogen bonds were formed between the Gln711(A) and Arg752(A) residues and the pyridine ring nitrogen atom, as well as between Leu704(A) and the nitrogen atom of the thiosemicarbazone core. In the **C5**-EGFR complex, Met769(A) participated in hydrogen bond formation with the pyridine ring nitrogen atom. Additionally, π–π stacking interactions were observed between the 2,4-dichlorophenyl substituents and the phenyl ring of Phe699(A). For validation purposes, the co-crystallized ligands present in the deposited protein structures were redocked into the active sites (Figures S35-S38), yielding higher docking scores in all four cases.

Table 5. Docking scores of **C1**-**C6** and reference inhibitors docked into the active sites of selected molecular targets. Docking scores are expressed as the total ChemPLP fitness values for each ligand-target complex. The values are presented as a heatmap, where green indicates the highest docking scores. Target PDB IDs are provided in parentheses.

Compound	Docking score			
	BRAF (3OG7)	hAR (2AM9)	EGFR (1M17)	PI3K (4JPS)
C1	56.44	44.30	52.25	55.85
C2	59.12	44.54	52.48	55.96
C3	60.28	38.37	52.89	57.01
C4	55.76	31.17	54.32	58.23
C5	56.92	30.40	55.12	61.10
C6	55.66	46.33	53.24	57.28
Inhibitor*	107.72 (0.4129)	76.81 (0.4126)	76.80 (1.9274)	91.19 (1.1852)

*Root mean square deviation (RMSD) values are given in parentheses for each reference inhibitor originally present in the deposited crystal structures of the molecular targets.

 doi:10.20944/preprints202604.0146.v1

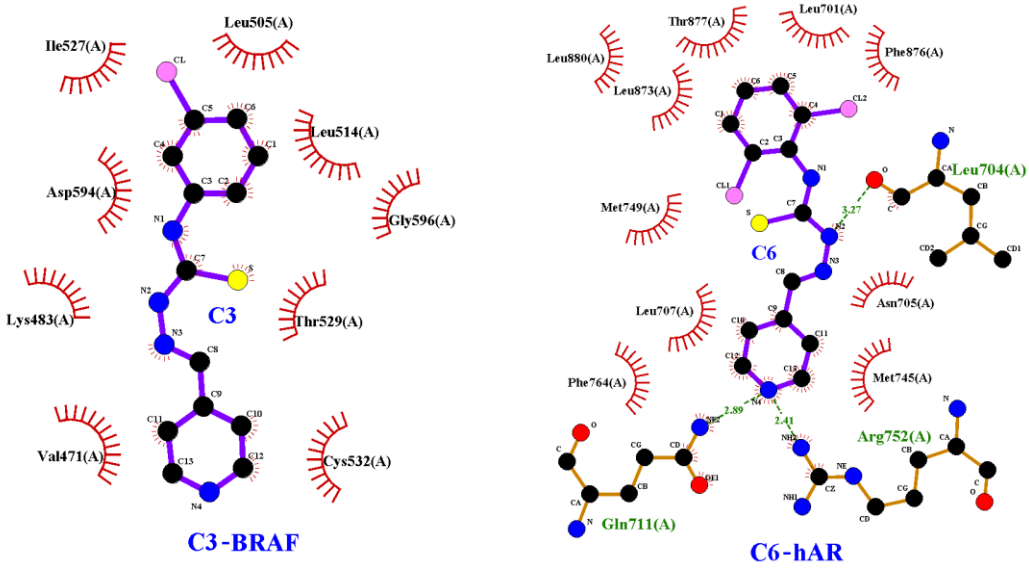

Figure 5. 2D representations of **C3**-BRAF and **C6**-hAR complexes. Green dashed lines represent hydrogen bonds, red arcs represent hydrophobic interactions.

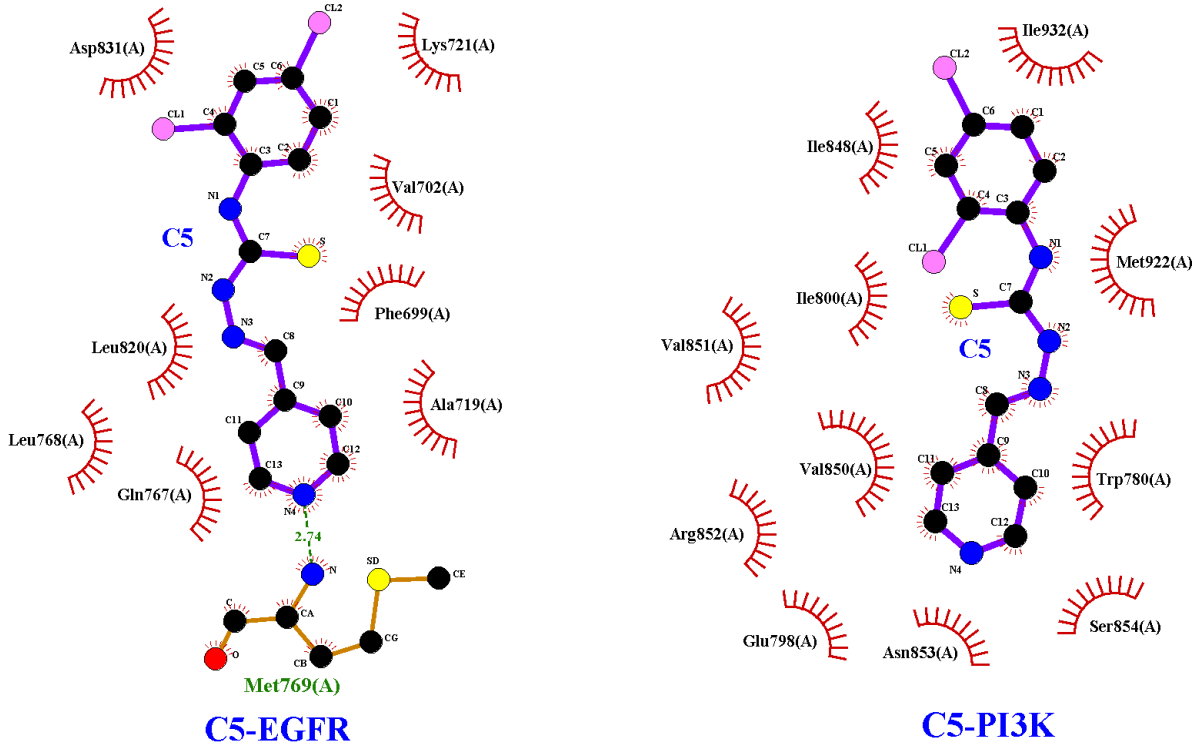

Figure 6. 2D representations of **C5**-EGFR and **C5**-PI3K complexes. Green dashed lines represent hydrogen bonds, red arcs represent hydrophobic interactions.

3. Materials and Methods

3.1. Chemicals and Synthesis

Chemicals used for the synthesis were purchased from the following companies: thiosemicarbazides and 4-pyridinecarboxaldehyde from Sigma-Aldrich (St. Louis, MO, USA), concentrated hydrochloric acid from Sigma-Aldrich, and methanol from POCH (Gliwice, Poland). The reagents were of chemically pure quality.

 doi:10.20944/preprints202604.0146.v1

Preparation of thiosemicarbazone derivatives: a solution of thiosemicarbazide (1 mmol) in methanol (20 mL) was slowly added to a solution of 4-pyridinecarboxaldehyde (1 mmol) and a few drops of 36% HCl. The resulting mixture was heated under reflux for 2 hours. The precipitate was then filtered off, washed with methanol, and recrystallized from methanol.

C1: N-phenyl-2-[(pyridin-4-yl)methylidene]hydrazine-1-carbothioamide

$C_{13}H_{12}N_4S$ (256.326 g/mol), yield: 83%, m.p. 73-75°C. **^{1}H NMR** (700 MHz, DMSO-d_6): δ 12.04 (s, 1H, NH), 10.25 (s, 1H, NH), 8.60 (d, 2H, *J* = 5.4 Hz, CH_{Py}), 8.09 (s, 1H, CH), 7.86 (d, 2H, *J* = 5.4 Hz, CH_{Py}), 7.53-7.20 (m, 5H, CH_{Ph}). **^{13}C NMR** (176 MHz, DMSO-d_6): δ 177.9, 150.5 (2C), 141.8, 140.5, 139.4, 128.6 (2C), 126.7 (2C), 126.1, 121.9 (2C). **ESI-MS** m/z: $[M+H]^+$ theoretical: 257.0855, measured: 257.0847. **FTIR** (cm^{-1}): ν(NH): 3300; ν(CH): 3130; ν(CC): 1595, 1529; ν(CN), δ(CH), δ(NH): 1446, 1262, 1190, 1101, 998, 910, 870, 744, 691.

C2: N-(2-chlorophenyl)-2-[(pyridin-4-yl)methylidene]hydrazine-1-carbothioamide

$C_{13}H_{11}N_4SCl$ (290.771 g/mol), yield: 81%, m.p. 180-184°C. **^{1}H NMR** (700 MHz, DMSO-d_6): δ 12.20 (s, 1H, NH), 10.23 (s, 1H, NH), 8.61-8.60 (m, 2H, CH_{Py}), 8.10 (s, 1H, CH), 7.84-7.83 (m, 2H, CH_{Py}), 7.60 (dd, 1H, *J* = 7.8 Hz, 1.5 Hz, CH_{Ph}), 7.54 (dd, 1H, *J* = 7.8 Hz, 1.5 Hz, CH_{Ph}), 7. 38 (dt, 1H, *J* = 7.8 Hz, 1.5 Hz, CH_{Ph}), 7.32 (dt, 1H, *J* = 7.8 Hz, 1.5 Hz, CH_{Ph}). **^{13}C NMR** (176 MHz, DMSO-d_6): δ 177.9, 150.5 (2C), 141.3, 140.6, 136.9, 131.7, 130.8, 129.9, 128.7, 127.7, 121.8 (2C). **ESI-MS** m/z: $[M+H]^+$ theoretical: 291.0466, measured: 291.0457. **FTIR** (cm^{-1}): ν(NH): 3316, 3258, 3149; ν(CH): 2988; ν(CC): 1596, 1550; ν(CN), δ(CH), δ(NH): 1443, 1420, 1266, 1191, 1095, 927; ν(CN), δ(CH), ν(CCl): 811, 752.

C3: N-(3-chlorophenyl)-2-[(pyridin-4-yl)methylidene]hydrazine-1-carbothioamide

$C_{13}H_{11}N_4SCl$ (290.771 g/mol), yield: 82%, m.p. 186-190°C. **^{1}H NMR** (700 MHz, DMSO-d_6): δ 12.18 (s, 1H, NH), 10.30 (s, 1H, NH), 8.62-8.61 (m, 2H, CH_{Py}), 8.11 (s, 1H, CH), 7.87-7.86 (m, 2H, CH_{Py}), 7.71 (t, 1H, *J* = 2.0 Hz, CH_{Ph}), 7.57 (ddd, 1H, *J* = 8.0 Hz, 2.0 Hz, 0.9 Hz, CH_{Ph}), 7.39 (t, 1H, *J* = 8.0 Hz, CH_{Ph}), 7.27 (ddd, 1H, *J* = 8.0 Hz, 2.0 Hz, 0.9 Hz, CH_{Ph}). **^{13}C NMR** (176 MHz, DMSO-d_6): δ 176.9, 150.5 (2C), 141.6, 141.0, 140.9, 132.7, 130.1, 125.9, 125.8, 124.9, 121.9 (2C). **ESI-MS** m/z: $[M+H]^+$ theoretical: 291.0466, measured: 291.0457. **FTIR** (cm^{-1}): ν(NH): 3331; ν(CH): 3126; ν(CC): 1587, 1552, 1523; ν(CN), δ(CH), δ(NH): 1416, 1282, 1195, 1101, 1076, 961, 927; ν(CN), δ(CH), ν(CCl): 772; δ(CH), ν(CCl): 692.

C4: N-(4-chlorophenyl)-2-[(pyridin-4-yl)methylidene]hydrazine-1-carbothioamide

$C_{13}H_{11}N_4SCl$ (290.771 g/mol), yield: 74%, m.p. 207-209°C. **^{1}H NMR** (700 MHz, DMSO-d_6): δ 12.15 (s, 1H, NH), 10.30 (s, 1H, NH), 8.64-8.63 (m, 2H, CH_{Py}), 8.13 (s, 1H, CH), 7.88-7.87 (m, 2H, CH_{Py}), 7.61-7.43 (m, 4H, CH_{Ph}). **^{13}C NMR** (176 MHz, DMSO-d_6): δ 176.6, 150.0 (2C), 141.2, 140.4, 137.9, 129.6, 128.0 (2C), 127.7 (2C), 121.4 (2C). **ESI-MS** m/z: $[M+H]^+$ theoretical: 291.0466, measured: 291.0458. **FTIR** (cm^{-1}): ν(NH): 3300; ν(CC): 1591, 1533; ν(CN), δ(CH), δ(NH): 1489, 1388, 1303, 1258, 1188, 998, 921; ν(CN), δ(CH), ν(CCl): 827, 761.

C5: N-(2,4-dichlorophenyl)-2-[(pyridin-4-yl)methylidene]hydrazine-1-carbothioamide

$C_{13}H_{10}N_4SCl_2$ (325.261 g/mol), yield: 82%, m.p. 216-218°C. **^{1}H NMR** (700 MHz, DMSO-d_6): δ 12.28 (s, 1H, NH), 10.24 (s, 1H, NH), 8.63-8.62 (m, 2H, CH_{Py}), 8.12 (s, 1H, CH), 7.86-7.85 (m, 2H, CH_{Py}), 7.74 (d, 1H, *J* = 2.4 Hz, CH_{Ph}), 7.62 (d, 1H, *J* = 8.5 Hz, CH_{Ph}), 7.48 (dd, 1H, *J* = 8.5 Hz, 2.4 Hz, CH_{Ph}). **^{13}C NMR** (176 MHz, DMSO-d_6): δ 178.5, 150.1 (2C), 141.1, 140.4, 135.8, 132.5, 131.7, 131.65, 128.9, 127.4, 121.3 (2C). **ESI-MS** m/z: $[M+H]^+$ theoretical: 325.0076, measured: 325.0069. **FTIR** (cm^{-1}): ν(NH): 3266; ν(CC): 1579, 1529; ν(CN), δ(CH), δ(NH): 1379, 1315, 1255, 1185, 1101, 998; ν(CN), δ(CH), ν(CCl): 802.

C6: N-(2,6-dichlorophenyl)-2-[(pyridin-4-yl)methylidene]hydrazine-1-carbothioamide

$C_{13}H_{10}N_4SCl_2$ (325.261 g/mol), yield: 79%, m.p. 185-188°C. **^{1}H NMR** (700 MHz, DMSO-d_6): δ 12.24 (s, 1H, NH), 10.25 (s, 1H, NH), 8.61-8.60 (m, 2H, CH_{Py}), 8.09 (s, 1H, CH), 7.86-7.85 (m, 2H, CH_{Py}), 7.55 (d, 2H, *J* = 8.1 Hz, CH_{Ph}), 7.38 (t, 1H, *J* = 8.1 Hz, CH_{Ph}). **^{13}C NMR** (176 MHz, DMSO-d_6): δ 177.8, 150.0 (2C), 141.2, 140.2, 135.1 (2C), 134.9, 129.5, 128.4 (2C), 121.3 (2C). **ESI-MS** m/z: $[M+H]^+$ theoretical: 325.0076, measured: 325.0068. **FTIR** (cm^{-1}): ν(NH): 3330, 3222; ν(CC): 1561, 1505; ν(CN), δ(CH), δ(NH): 1270, 1222, 1199, 1103, 1014, 927, 870; ν(CN), δ(CH), ν(CCl): 815, 778.

3.2. NMR Spectroscopy

 doi:10.20944/preprints202604.0146.v1

NMR spectra were acquired on a Bruker Ultra Shield 700 instrument, running at room temperature at 700 MHz for ^{1}H and 176 MHz for ^{13}C, respectively. Chemical shifts (δ) are reported in ppm relative to residual solvent signals (DMSO-d_6: 2.50 ppm for 1H NMR, 39.52 ppm for ^{13}C NMR).

3.3. Mass Spectrometry

An Exploris 240 (Thermo Scientific, Germany, Bremen) mass spectrometer equipped with an electrospray ionization source was used. Positive-ion electrospray was performed at a spray voltage of 3.4 kV. Spectral acquisition was performed between m/z 80 and 800 in full scan mode. Data were analyzed using FreeStyle 1.8 (Thermo Scientific, USA) software. Samples were dissolved and diluted in methanol to achieve a concentration of 1 μg/mL. The Ultimate 3000 system (Thermo Scientific, Germany, Bremen) was then used to inject 1 μL of each sample at a flow rate of 20 μL/min.

3.4. Infrared Spectroscopy

FTIR spectra were recorded with an IR Tracer-100 Shimadzu Spectrometer (4000-600 cm^{-1} with recording accuracy of 1 cm^{-1}, Shimadzu, Kyoto, Japan) using KBr pellets prepared from KBr ground with the addition of the investigated sample.

3.5. Single-Crystal X-Ray Diffraction

The single-crystal X-ray diffraction data for **C6** were collected on the XtaLAB Synergy Dualflex Pilatus 300K diffractometer. Data collection, cell refinement, data reduction, and absorption correction were carried out using CrysAlisPro software [49]. The SHELXT [50] and SHELXL [51] programs implemented in Olex2 software [52] were used to solve and refine the structure. All non-hydrogen atoms were refined anisotropically. The carbon-bonded hydrogen atoms were positioned geometrically and refined using the riding model, whereas the nitrogen-bonded hydrogen atoms were located from the Fourier difference map and refined freely. Structural visualizations were made using the Mercury 2024.2.0 [53]. Geometrical parameters were calculated using the Platon PWT 2021.2 [54]. Crystal data and structure refinement details are summarized in Table 5. CCDC 2442569 contains the supplementary crystallographic data for **C6**. These data can be obtained free of charge via www.ccdc.cam.ac.uk/data_request/cif, or by emailing data_ request@ccdc.cam.ac.uk, or by contacting The Cambridge Crystallographic Data Centre, 12 Union Road, Cambridge CB2 1EZ, UK; fax: +44 1223 336033.

Table 5. Crystal data and structure refinement details for **C6**.

Empirical formula	$C_{15}H_{16}N_4OS_2Cl_2$
Formula weight	403.34
Temperature (K)	100.00(10)
Crystal system	orthorhombic
Space group	$P2_12_12_1$
a (Å)	8.25920(10)
b (Å)	8.64490(10)
c (Å)	25.9037(2)
α (°)	90
β (°)	90
γ (°)	90
Volume ($Å^3$)	1849.52(3)
Z	4
ϱcalc (g/cm^3)	1.448
μ (mm^{-1})	5.358
F(000)	832.0
Crystal size (mm^3)	0.14 × 0.08 × 0.06

 doi:10.20944/preprints202604.0146.v1

Radiation	Cu Kα (λ = 1.54184)
2θ range for data collect. (°)	6.824 to 159.422
Index ranges	-7 ≤ h ≤ 10, -10 ≤ k ≤ 10, -33 ≤ l ≤ 29
Reflections collected / independent	18368 / 3838
R_{int}	0.0288
Data/restraints/parameters	3838/0/225
Goodness-of-fit on F^2	1.108
Final R indexes [I>2s(I)]	R_1 = 0.0219, wR_2 = 0.0561
R indexes (all data)	R_1 = 0.0233, wR_2 = 0.0601
Largest diff. peak and hole (e•Å^{-3})	0.26/-0.18
Flack parameter	-0.015(9)

3.6. Antioxidant Activity

ABTS

To test the antioxidant activity of the obtained compounds, 2,2′-azino-bis(3-ethylbenzothiazoline-6-sulfonic acid) - ABTS (Merck, Steinheim, Germany) was used. Potassium persulfate ($K_2S_2O_8$, Merck, Steinheim, Germany) activates ABTS and converts it from the inactive to the active radical form. 6-hydroxy-2,5,7,8-tetramethylchroman-2-carboxylic acid (Trolox, Merck, Steinheim, Germany) was used as the standard. 19.20 mg of ABTS was weighed and dissolved in 5 mL of distilled water to obtain a 7 mM solution. To 5 mL of the ABTS solution, 88 µL of 140 mM potassium persulfate was added to generate the $ABTS^+$ cation radical. The mixture was protected from light and set aside at room temperature for 16 h. All tests were performed in 75 mM phosphate buffer (pH 7.4) with a final reaction volume of 100 µL per well. Compounds were first dissolved in dimethyl sulfoxide (DMSO, Merck, Steinheim, Germany) and then diluted in phosphate buffer to final concentrations of 0.01-25 µg/mL, as was Trolox. For the assay, 50 µL of the compound or Trolox solution and 50 µL of $ABTS^+$ solution were added to wells of a 96-well plate (Greiner Bio-One, Frickenhausen, Germany). Absorbance was immediately measured at 734 nm at room temperature using a Synergy H1 multifunctional plate reader (BioTek). 75 mM phosphate buffer (pH 7.4) was used as a blank. The plate was automatically shaken for 5 s before each measurement. All tests were performed in triplicate. Percent inhibition of $ABTS^+$ was plotted against compound concentration, and IC_{50} values were calculated from the linear regression equation [55]:

$$y = ax + b;\ IC_{50} = \frac{50 - b}{a}$$

DPPH

The antioxidant activity of compounds was measured using 2,2-diphenyl-1-picrylhydrazyl (DPPH, Merck, Steinheim, Germany) as the oxidizing agent. 6-hydroxy-2,5,7,8-tetramethylchroman-2-carboxylic acid (Trolox, Merck, Steinheim, Germany) was used as the standard. The assays and standard were dissolved in 75 mM phosphate buffer (pH 7.4) with a final reaction volume of 50 µL per well of a 96-well plate. 1.58 mg of DPPH was weighed and dissolved in 20 mL of methanol to obtain a 0.2 mM solution. All compounds and the standard were first dissolved in dimethyl sulfoxide (DMSO, Merck, Steinheim, Germany) and then diluted in phosphate buffer. Final concentrations were 0.01-25 µg/mL for both Trolox and all compounds. Solutions of the tested compounds (50 µL) and DPPH solution (50 µL) were added to the appropriate wells of a 96-well microplate (Greiner Bio-One, Frickenhausen, Germany), giving a final volume of 100 µL per well. Plates were immediately placed in a multifunctional microplate reader Synergy H1 (BioTek), and absorbance was measured at 517 nm at room temperature. 75 mM phosphate buffer (pH 7.4) was used as a blank. The plate was automatically shaken for 5 s before each measurement. All tests were performed in triplicate. Percent inhibition of DPPH was plotted against compound concentration, and IC_{50} values were calculated from the linear regression equation [56]:

 doi:10.20944/preprints202604.0146.v1

$$y = ax + b;\ IC_{50} = \frac{50 - b}{a}$$

ORAC-FL

Oxygen Radical Absorbance Capacity-Fluorescein (ORAC-FL) was used to assess antioxidant activity of the compounds, with Trolox as a standard. Fluorescein disodium salt (FL, Merck, Steinheim, Germany), 2,2′-azobis(2-methylpropionamidine) dihydrochloride (APPH, Merck, Steinheim, Germany), and Trolox (Merck, Steinheim, Germany) were used. APPH solution was prepared as follows: 2 mg of fluorescein disodium was dissolved in 4.58 mL of PBS to obtain 1.17 mM. 3 µL of the fluorescein stock was diluted with 30 mL of PBS to obtain 117 nM. All compounds and Trolox were prepared in 75 mM phosphate buffer (pH 7.4) with a final mixture volume of 200 µL. The final concentrations of the tested compounds were 1-13 µM. Mixtures were incubated in the dark at 37℃ for 15 min. Plates were then placed in a multifunctional microplate reader Synergy H1 (BioTek), and fluorescence was measured kinetically at 70 s intervals for 140 min at 37℃, with excitation at 485 nm and emission at 520 nm. Phosphate buffer (pH 7.4) was used as a blank. The plate was automatically shaken for 10 s before each measurement. All tests were performed in triplicate. Percent effect (% NET AUC) was plotted against concentration. Linear regression was performed using:

$$y = ax + b$$

The Trolox equivalent (TE) was calculated as [57]:

$$TE = \frac{a}{a'}$$

where a is the slope of the tested compound and a' is the slope of the Trolox standard.

3.7. Anticancer Activity

Cell Culture

Human normal skin fibroblasts (BJ) and human cancer cell lines including melanoma (A375 and G-361), prostate cancer (LNCaP), colorectal cancer (Caco-2) and glioblastoma (U-87 MG) were obtained from the American Type Culture Collection (ATCC, Manassas, VA, USA). Cells were cultured as adherent monolayers in media recommended by ATCC. A375 cells were maintained in Dulbecco's Modified Eagle Medium DMEM (Corning Inc., Tewksbury, MA, USA), G-361 cells in McCoy's 5A medium (Corning Inc., Tewksbury, MA, USA), Caco-2, U-87 MG, and BJ cells in Eagle's Minimum Essential Medium EMEM (Corning Inc., Tewksbury, MA, USA) and LNCaP cells in RPMI-1640 medium (Corning Inc., Tewksbury, MA, USA). All media were supplemented with 10% (v/v) heat-inactivated fetal bovine serum (FBS) (Corning Inc., Tewksbury, MA, USA), penicillin (100 U/mL), streptomycin (100 µg/mL) and amphotericin B (0.25 µg/mL) (Sigma-Aldrich Chemicals, St. Louis, MO, USA). Cells were incubated at 37℃ in a humidified atmosphere containing 5% CO_2 and routinely passaged at approximately 80% confluence to maintain logarithmic growth. Cell detachment was performed using 0.25% trypsin-EDTA (Corning Inc., Tewksbury, MA, USA). Cell number and viability were determined by trypan blue exclusion using a Countess™ Automated Cell Counter (Thermo Fisher Scientific, Waltham, MA, USA). Cells between passages 5 and 10 were used in all experiments.

MTT Cytotoxicity Assay

The cytotoxic activity of compounds **C1**-**C6** was evaluated against the cancer cell lines and the normal BJ cell line using the MTT colorimetric assay (Sigma-Aldrich, USA). Cells were seeded into 96-well plates at a density of 2×10^4 cells per well and allowed to attach for 24 h. Subsequently cells were treated with the tested compounds at concentrations of 1, 25, 50, 75, and 100 µM and incubated for an additional 48 h. After treatment MTT solution was added to each well at a final concentration of 0.5 mg/mL and incubated for 4 h at 37℃. The medium was then removed, and the formazan crystals

 doi:10.20944/preprints202604.0146.v1

were dissolved in dimethyl sulfoxide (DMSO) (POCH, Gliwice, Poland). Absorbance was measured at 570 nm using a PowerWave microplate spectrophotometer (BioTek Instruments, USA). Cell viability was expressed as a percentage of untreated control cells. All experiments were performed in triplicate and repeated three times independently. IC_{50} values were determined by nonlinear regression analysis using GraphPad Prism (GraphPad Software, San Diego, CA). Dose-response curves were fitted using a four-parameter logistic model with the top and bottom plateaus constrained to 100% and 0% cell viability, respectively.

3.8. Antibacterial Activity

The antimicrobial activity of the synthesized compounds was evaluated by determining the MIC using the agar well diffusion method. The MICs of the tested samples were determined against a panel of reference microorganisms obtained from the American Type Culture Collection (ATCC), including Gram-negative bacteria (*Escherichia coli* ATCC 10530, *Salmonella Typhimurium* ATCC 14028), and Gram-positive bacteria (*Staphylococcus aureus* ATCC 25923, *Staphylococcus aureus* ATCC 6538, *Staphylococcus epidermidis* ATCC 12228, *Enterococcus faecalis* ATCC 29212, *Listeria monocytogenes* ATCC 19115, *Bacillus subtilis* ATCC 6633), as well as *Bacillus cereus* ŁOCK 0807, obtained from the Pure Culture of Industrial Microorganisms of the Institute of Fermentation Technology and Microbiology ŁOCK 105 (Łódź, Poland). The reference positive controls used in this study were antibiotics: vancomycin for Gram-positive bacteria and ciprofloxacin for Gram-negative bacteria (*Escherichia coli*, *Salmonella Typhimurium*), purchased from Sigma-Aldrich, Saint Louis, MO, USA. Bacterial cultures grown for 24 h and adjusted to a density of 1.5×10^8 CFU/mL (corresponding to a 0.5 McFarland standard) were plated (0.1 mL) on Mueller–Hinton Agar (Merck, Darmstadt, Germany) following the procedures recommended by the European Committee on Antimicrobial Susceptibility Testing (EUCAST) [58]. Wells with a diameter of 8 mm were cut in the agar medium. Subsequently, 100 µL of prepared solutions containing the tested compounds at concentrations ranging from 10,000 mg/L to 1 mg/L dissolved in a 50% (v/v) DMSO were added to each well. The possible effect of the solvent was accounted for by including appropriate solvent controls. The plates were incubated at 30°C (for *B. subtilis* and *B. cereus*) or 37°C (for other bacteria) for 18 h. After incubation, the MIC value (the lowest concentration of the tested compounds that prevents bacterial growth) was determined and expressed in mg/L. The experiment was conducted in triplicate.

3.9. ADME Analysis

The pharmacokinetic profile of **C1**-**C6** compounds were evaluated using freely available online tools, the SwissADME service (Swiss Institute of Bioinformatics 2021) [59,60].

3.10. Molecular Docking

Molecular docking was performed using GOLD and Hermes software [61–63]. The crystal structures of the selected target molecules were obtained from Protein Data Bank: B-Raf Kinase V600E (BRAF; PDB ID: 3OG7 [64]), human Androgen Receptor (hAR; PDB ID: 2AM9 [65]), Epidermal Growth Factor Receptor (EGFR; PDB ID: 1M17 [66]), and Lipid Kinase PI3K alpha (PI3K; PDB ID: 4JPS [67]). All ligands were optimized with Gaussian software using B3LYP/6-31G method [68]. Before docking, the water molecules and bound ligands were removed and hydrogen atoms were added. The binding properties were calculated with ChemPLP scoring function for the area within a radius of 6.0 Å from the original ligands. All ligands were set as flexible molecules. The results were visualized using Hermes 2023.2.0 and LigPlot + v.2.3.1 software [69,70].

4. Conclusions

In this study, six 4-pyridyl-based thiosemicarbazones variously substituted with chlorine atoms were synthesized, and their biological potential was thoroughly evaluated. All compounds possess favourable pharmacokinetic profiles and can potentially be utilized as drugs. While the antimicrobial

 doi:10.20944/preprints202604.0146.v1

activity of the tested compounds was negligible, some of them exhibited potent antioxidant and anticancer activity. In general, compounds with double chlorine substitution (**C5** and **C6**) showed stronger radical scavenging capacity than the unsubstituted (**C1**) and mono-chlorinated (**C2**-**C4**) derivatives, with **C6** consistently displaying the highest activity. These results indicate that chlorination enhances the antioxidant potential of the thiosemicarbazone scaffold, with structural modifications providing a means to tune radical scavenging properties. Interestingly, compound **C2** exhibited the strongest anticancer activity, indicating that the mechanisms underlying cytotoxicity differ from those driving radical scavenging and that structural features other than chlorination contribute to anticancer efficacy. The lowest IC_{50} values were observed against LNCaP prostate cancer cells (53.85 ± 0.83 μM) and A375 skin cancer cells (76.80 ± 7.62 μM). Importantly, the same compound was significantly less toxic toward healthy BJ cells, with 90.26% viability observed at the highest tested concentration (100 μM). These results highlight the strong selectivity and tunability of chlorinated thiosemicarbazones as potential drug candidates.

Supplementary Materials: The following supporting information can be downloaded at the website of this paper posted on Preprints.org.

Author Contributions: Conceptualization, M.P., P.S., A.C., B.R.; methodology, A.C., M.P., E.K.-B., M.S., and P.S.; software, A.R. and E.F.; formal analysis A.C., M.P., E.K.-B., M.S., B.R. and P.S.; investigation, A.R., E.F., B.R., M.Ś., A.G., S.Ś., M.S., and M.J.; data curation, A.R.; writing—A.C., A.R., P.S. and B.R.; writing—review and editing, A.C., A.R. and B.R.; visualization, A.R., E.F. and B.R.; supervision, A.C.; project administration, A.C.

Funding: The work was partially financed from the subsidy no 16.16.160.557 of the Polish Ministry of Science and Higher Education.

Data Availability Statement: Data is contained within the article or Supplementary Materials.

Acknowledgments: This article was completed while two authors, Ewelina Fornal and Bartłomiej Rogalewicz were Doctoral Candidates in the Interdisciplinary Doctoral School at the Lodz University of Technology, Poland.

Conflicts of Interest: The authors declare no conflicts of interest.

References

1. Hassan, A.A.; Shawky, A.M.; Shehatta, H.S. Chemistry and Heterocyclization of Thiosemicarbazones. *Journal of Heterocyclic Chemistry* **2012**, *49*, 21–37, doi:10.1002/jhet.677.
2. Prajapati, N.P.; Patel, H.D. Novel Thiosemicarbazone Derivatives and Their Metal Complexes: Recent Development. *Synthetic Communications* **2019**, *49*, 2767–2804, doi:10.1080/00397911.2019.1649432.
3. Rogalewicz, B.; Świątkowski, M.; Iwan, M.; Michalczuk, M.; Kubik, J.; Korga-Plewko, A.; Pitucha, M.; Gajda, A.; Ścieszka, S.; Kordialik-Bogacka, E.; et al. Structural Studies and Biological Activity of the New Ni(II), Cu(II), Zn(II), Pd(II), and Ag(I) Thiosemicarbazone-Based Complexes. *Journal of Inorganic Biochemistry* **2025**, *271*, 112962, doi:10.1016/j.jinorgbio.2025.112962.
4. Kizilcikli, İ.; Kurt, Y.D.; Akkurt, B.; Genel, A.Y.; Birteksöz, S.; Ötük, G.; Ülküseven, B. Antimicrobial Activity of a Series of Thiosemicarbazones and Their ZnII and PdII Complexes. *Folia Microbiol* **2007**, *52*, 15–25, doi:10.1007/BF02932132.
5. Mbah, J.A.; Ayimele, G.A.; Eyonganyoh, E.N.; Nfor, E.N. Synthesis, Molecular Structure and Antibacterial Activity of Benzylmethyl-4-Methyl-3-Thiosemicarbazone. *International Journal of Organic Chemistry* **2017**, *7*, 83–90, doi:10.4236/ijoc.2017.72007.
6. Finch, R.A.; Liu, M.; Grill, S.P.; Rose, W.C.; Loomis, R.; Vasquez, K.M.; Cheng, Y.; Sartorelli, A.C. Triapine (3-Aminopyridine-2-Carboxaldehyde- Thiosemicarbazone): A Potent Inhibitor of Ribonucleotide Reductase Activity with Broad Spectrum Antitumor Activity. *Biochem Pharmacol* **2000**, *59*, 983–991, doi:10.1016/s0006-2952(99)00419-0.
7. Finch, R.A.; Liu, M.-C.; Cory, A.H.; Cory, J.G.; Sartorelli, A.C. Triapine (3-Aminopyridine-2-Carboxaldehyde Thiosemicarbazone; 3-AP): An Inhibitor of Ribonucleotide Reductase with Antineoplastic Activity. *Advances in Enzyme Regulation* **1999**, *39*, 3–12, doi:10.1016/S0065-2571(98)00017-X.

 doi:10.20944/preprints202604.0146.v1

8. Niso, M.; Kopecka, J.; Abatematteo, F.S.; Berardi, F.; Riganti, C.; Abate, C. Multifunctional Thiosemicarbazones Targeting Sigma Receptors: In Vitro and in Vivo Antitumor Activities in Pancreatic Cancer Models. *Cell Oncol.* **2021**, *44*, 1307–1323, doi:10.1007/s13402-021-00638-5.
9. El Majzoub, R.; Fayyad-kazan, M.; Nasr El Dine, A.; Makki, R.; Hamade, E.; Grée, R.; Hachem, A.; Talhouk, R.; Fayyad-Kazan, H.; Badran, B. A Thiosemicarbazone Derivative Induces Triple Negative Breast Cancer Cell Apoptosis: Possible Role of miRNA-125a-5p and miRNA-181a-5p. *Genes Genom* **2019**, *41*, 1431–1443, doi:10.1007/s13258-019-00866-y.
10. Bai, C.; Wu, S.; Ren, S.; Zhu, M.; Luo, G.; Xiang, H. Synthesis and Evaluation of Novel Thiosemicarbazone and Semicarbazone Analogs with Both Anti-Proliferative and Anti-Metastatic Activities against Triple Negative Breast Cancer. *Bioorganic & Medicinal Chemistry* **2021**, *37*, 116107, doi:10.1016/j.bmc.2021.116107.
11. Sever, B.; Çiftçi, G.A.; Özdemir, A.; Altıntop, M.D. Design, Synthesis and Biological Evaluation of New Bis(Thiosemicarbazone) Derivatives as Potential Targeted Anticancer Agents for Non-Small Cell Lung Cancer. *J. Res. Pharm.* **2025**, *24*, 670–680, doi:10.35333/jrp.2020.222.
12. Kunos, C.A.; Radivoyevitch, T.; Waggoner, S.; Debernardo, R.; Zanotti, K.; Resnick, K.; Fusco, N.; Adams, R.; Redline, R.; Faulhaber, P.; et al. Radiochemotherapy plus 3-Aminopyridine-2-Carboxaldehyde Thiosemicarbazone (3-AP, NSC #663249) in Advanced-Stage Cervical and Vaginal Cancers. *Gynecologic Oncology* **2013**, *130*, 75–80, doi:10.1016/j.ygyno.2013.04.019.
13. Kunos, C.A.; Waggoner, S.; von Gruenigen, V.; Eldermire, E.; Pink, J.; Dowlati, A.; Kinsella, T.J. Phase I Trial of Pelvic Radiation, Weekly Cisplatin, and 3-Aminopyridine-2-Carboxaldehyde Thiosemicarbazone (3-AP, NSC #663249) for Locally Advanced Cervical Cancer. *Clin Cancer Res* **2010**, *16*, 1298–1306, doi:10.1158/1078-0432.CCR-09-2469.
14. He, Z.-X.; Huo, J.-L.; Gong, Y.-P.; An, Q.; Zhang, X.; Qiao, H.; Yang, F.-F.; Zhang, X.-H.; Jiao, L.-M.; Liu, H.-M.; et al. Design, Synthesis and Biological Evaluation of Novel Thiosemicarbazone-Indole Derivatives Targeting Prostate Cancer Cells. *European Journal of Medicinal Chemistry* **2021**, *210*, 112970, doi:10.1016/j.ejmech.2020.112970.
15. Altintop, M.D.; Sever, B.; Özdemir, A.; Kuş, G.; Oztopcu-Vatan, P.; Kabadere, S.; Kaplancikli, Z.A. Synthesis and Evaluation of Naphthalene-Based Thiosemicarbazone Derivatives as New Anticancer Agents against LNCaP Prostate Cancer Cells. *Journal of Enzyme Inhibition and Medicinal Chemistry* **2016**, *31*, 410–416, doi:10.3109/14756366.2015.1031126.
16. Shahi, N.; Yadav, P.N.; Chaudhary, U.; Saad, M.; Mahiya, K.; Khan, A.; Shafi, S.; Pokharel, Y.R. 5-Methoxyisatin N(4)-Pyrrolidinyl Thiosemicarbazone (MeOIstPyrd) Restores Mutant P53 and Inhibits the Growth of Skin Cancer Cells, In Vitro. *ACS Omega* **2023**, *8*, 31998–32016, doi:10.1021/acsomega.3c03824.
17. Cancer Tomorrow Available online: https://gco.iarc.who.int/today/ (accessed on 18 February 2026).
18. Murray, C.J.L.; Sharara, F.; Swetschinski, L.; Aguilar, G.R.; Gray, A.; Han, C.; Bisignano, C.; Rao, P.; Wool, E.; Johnson, S.C.; et al. Global Burden of Bacterial Antimicrobial Resistance in 2019: A Systematic Analysis. *The Lancet* **2022**, *399*, 629–655, doi:10.1016/S0140-6736(21)02724-0.
19. Shakya, B.; Yadav, P.N. Thiosemicarbazones as Potent Anticancer Agents and Their Modes of Action. *Mini-Reviews in Medicinal Chemistry 20*, 638–661, doi:10.2174/1389557519666191029130310.
20. Synnott, N.C.; O'Connell, D.; Crown, J.; Duffy, M.J. COTI-2 Reactivates Mutant P53 and Inhibits Growth of Triple-Negative Breast Cancer Cells. *Breast Cancer Res Treat* **2020**, *179*, 47–56, doi:10.1007/s10549-019-05435-1.
21. Quach, P.; Gutierrez, E.; Basha, M.T.; Kalinowski, D.S.; Sharpe, P.C.; Lovejoy, D.B.; Bernhardt, P.V.; Jansson, P.J.; Richardson, D.R. Methemoglobin Formation by Triapine, Di-2-Pyridylketone-4,4-Dimethyl-3-Thiosemicarbazone (Dp44mT), and Other Anticancer Thiosemicarbazones: Identification of Novel Thiosemicarbazones and Therapeutics That Prevent This Effect. *Molecular Pharmacology* **2012**, *82*, 105–114, doi:10.1124/mol.112.078964.
22. Rogalewicz, B.; Iwan, M.; Świątkowski, M.; Michalczuk, M.; Kubik, J.; Humeniuk, E.; Korga-Plewko, A.; Pitucha, M.; Boruta, T.; Ścieszka, S.; et al. Structure-Activity Relationship of Cu(II) and Pd(II) Thiosemicarbazone Complexes with Anticancer and Antibacterial Properties. *ChemRxiv 2025*, doi:10.26434/chemrxiv-2025-p1fdc.

 doi:10.20944/preprints202604.0146.v1

23. Joshi, S.; Srivastava, R. Effect of "Magic Chlorine" in Drug Discovery: An in Silico Approach. *RSC Adv.* **2023**, *13*, 34922–34934, doi:10.1039/D3RA06638J.
24. Chiodi, D.; Ishihara, Y. "Magic Chloro": Profound Effects of the Chlorine Atom in Drug Discovery. *J. Med. Chem.* **2023**, *66*, 5305–5331, doi:10.1021/acs.jmedchem.2c02015.
25. Vlad, I.M.; Nuță, D.C.; Ancuceanu, R.V.; Caproiou, M.T.; Dumitrascu, F.; Marinas, I.C.; Chifiriuc, M.C.; Măruţescu, L.G.; Zarafu, I.; Papacocea, I.R.; et al. New O-Aryl-Carbamoyl-Oxymino-Fluorene Derivatives with MI-Crobicidal and Antibiofilm Activity Enhanced by Combination with Iron Oxide Nanoparticles. *Molecules* **2021**, *26*, 3002, doi:10.3390/molecules26103002.
26. Hassanzadeh, F.; Jafari, E.; Hakimelahi, G.H.; Khajouei, M.R.; Jalali, M.; Khodarahmi, G.A. Antibacterial, Antifungal and Cytotoxic Evaluation of Some New Quinazolinone Derivatives. *Res Pharm Sci* **2012**, *7*, 87–94.
27. Demchenko, S.; Lesyk, R.; Yadlovskyi, O.; Zuegg, J.; Elliott, A.G.; Drapak, I.; Fedchenkova, Y.; Suvorova, Z.; Demchenko, A. Synthesis, Antibacterial and Antifungal Activity of New 3-Aryl-5H-Pyrrolo[1,2-a]Imidazole and 5H-Imidazo[1,2-a]Azepine Quaternary Salts. *Molecules* **2021**, *26*, 4253, doi:10.3390/molecules26144253.
28. Al-Mutairi, A.A.; Al-Alshaikh, M.A.; Al-Omary, F.A.M.; Hassan, H.M.; El-Mahdy, A.M.; El-Emam, A.A. Synthesis, Antimicrobial, and Anti-Proliferative Activities of Novel 4-(Adamantan-1-Yl)-1-Arylidene-3-Thiosemicarbazides, 4-Arylmethyl N′-(Adamantan-1-Yl)Piperidine-1-Carbothioimidates, and Related Derivatives. *Molecules* **2019**, *24*, 4308, doi:10.3390/molecules24234308.
29. Kawai, A.; Kobashigawa, Y.; Hirata, K.; Morioka, H.; Imoto, S.; Nishi, K.; Chuang, V.T.G.; Yamasaki, K.; Otagiri, M. Chlorine Atoms of an Aripiprazole Molecule Control the Geometry and Motion of Aripiprazole and Deschloro-Aripiprazole in Subdomain IIIA of Human Serum Albumin. *ACS Omega* **2022**, *7*, 29944–29951, doi:10.1021/acsomega.2c02929.
30. Naumann, K. Influence of Chlorine Substituents on Biological Activity of Chemicals: A Review. *Pest Management Science* **2000**, *56*, 3–21, doi:10.1002/(SICI)1526-4998(200001)56:1<3::AID-PS107>3.0.CO;2-P.
31. Naumann, K.; Cropscience, B. How Chlorine in Molecules Affects Biological Activity.; 2003.
32. Nagaoka, H.; Miyakoshi, T.; Kasuga, J.; Yamada, Y. Synthesis of a Halogenated Clavulone Analog. *Tetrahedron Letters* **1985**, *26*, 5053–5056, doi:10.1016/S0040-4039(01)80851-0.
33. Czylkowska, A.; Pitucha, M.; Raducka, A.; Fornal, E.; Kordialik-Bogacka, E.; Ścieszka, S.; Smoluch, M.; Burdan, F.; Jędrzejec, M.; Szymański, P. Thiosemicarbazone-Based Compounds: A Promising Scaffold for Developing Antibacterial, Antioxidant, and Anticancer Therapeutics. *Molecules* **2025**, *30*, 129, doi:10.3390/molecules30010129.
34. Cornea, A.C.; Marc, G.; Ionuț, I.; Moldovan, C.; Stana, A.; Oniga, S.D.; Pîrnău, A.; Vlase, L.; Oniga, I.; Oniga, O. Synthesis, Characterization, and Antioxidant Activity Evaluation of New N-Methyl Substituted Thiazole-Derived Polyphenolic Compounds. *Molecules* **2025**, *30*, 1345, doi:10.3390/molecules30061345.
35. Neacșu, S.M.; Mititelu, M.; Ozon, E.A.; Musuc, A.M.; Iuga, I.D.M.; Manolescu, B.N.; Petrescu, S.; Pandele Cusu, J.; Rusu, A.; Surdu, V.-A.; et al. Comprehensive Analysis of Novel Synergistic Antioxidant Formulations: Insights into Pharmacotechnical, Physical, Chemical, and Antioxidant Properties. *Pharmaceuticals* **2024**, *17*, 690, doi:10.3390/ph17060690.
36. Sharipova, G.M.; Safarova, I.V.; Khairullina, V.R.; Gerchikov, A.Y.; Zimin, Y.S.; Savchenko, R.G.; Limantseva, R.M. Kinetics and Mechanism of Antioxidant Action of Polysubstituted Tetrahydroquinolines in Liquid-Phase Oxidation Reactions of Organic Compounds by Oxygen. *International Journal of Chemical Kinetics* **2022**, *54*, 435–443, doi:10.1002/kin.21572.
37. Olicheva, V.; Beloborodov, V.; Sharifi, S.; Dubrovskaya, A.; Zhevlakova, A.; Selivanova, I.; Ilyasov, I. Dihydroquercetin and Related Flavonoids in Antioxidant Formulations with α-Tocopherol. *International Journal of Molecular Sciences* **2025**, *26*, 5659, doi:10.3390/ijms26125659.
38. Luo, M.; Zhou, L.; Huang, Z.; Li, B.; Nice, E.C.; Xu, J.; Huang, C. Antioxidant Therapy in Cancer: Rationale and Progress. *Antioxidants* **2022**, *11*, 1128, doi:10.3390/antiox11061128.
39. Antioxidants and Cancer | Health and Medicine | Research Starters | EBSCO Research Available online: https://www.ebsco.com (accessed on 17 February 2026).

 doi:10.20944/preprints202604.0146.v1

40. Lipinski, C.A.; Lombardo, F.; Dominy, B.W.; Feeney, P.J. Experimental and Computational Approaches to Estimate Solubility and Permeability in Drug Discovery and Development settings1PII of Original Article: S0169-409X(96)00423-1. The Article Was Originally Published in Advanced Drug Delivery Reviews 23 (1997) 3–25.1. *Advanced Drug Delivery Reviews* **2001**, *46*, 3–26, doi:10.1016/S0169-409X(00)00129-0.
41. Ghose, A.K.; Viswanadhan, V.N.; Wendoloski, J.J. A Knowledge-Based Approach in Designing Combinatorial or Medicinal Chemistry Libraries for Drug Discovery. 1. A Qualitative and Quantitative Characterization of Known Drug Databases. *J. Comb. Chem.* **1999**, *1*, 55–68, doi:10.1021/cc9800071.
42. Veber, D.F.; Johnson, S.R.; Cheng, H.-Y.; Smith, B.R.; Ward, K.W.; Kopple, K.D. Molecular Properties That Influence the Oral Bioavailability of Drug Candidates. *J. Med. Chem.* **2002**, *45*, 2615–2623, doi:10.1021/jm020017n.
43. Egan, W.J.; Merz, Kenneth M.; Baldwin, J.J. Prediction of Drug Absorption Using Multivariate Statistics. *J. Med. Chem.* **2000**, *43*, 3867–3877, doi:10.1021/jm000292e.
44. Muegge, I.; Heald, S.L.; Brittelli, D. Simple Selection Criteria for Drug-like Chemical Matter. *J. Med. Chem.* **2001**, *44*, 1841–1846, doi:10.1021/jm015507e.
45. Kozyra, P.; Pitucha, M. Revisiting the Role of B-RAF Kinase as a Therapeutic Target in Melanoma. *Curr Med Chem* **2024**, *31*, 2003–2020, doi:10.2174/0109298673258495231011065225.
46. Fujita, K.; Nonomura, N. Role of Androgen Receptor in Prostate Cancer: A Review. *World J Mens Health* **2019**, *37*, 288–295, doi:10.5534/wjmh.180040.
47. Xu, H.; Zong, H.; Ma, C.; Ming, X.; Shang, M.; Li, K.; He, X.; Du, H.; Cao, L. Epidermal Growth Factor Receptor in Glioblastoma. *Oncol Lett* **2017**, *14*, 512–516, doi:10.3892/ol.2017.6221.
48. He, Y.; Sun, M.M.; Zhang, G.G.; Yang, J.; Chen, K.S.; Xu, W.W.; Li, B. Targeting PI3K/Akt Signal Transduction for Cancer Therapy. *Sig Transduct Target Ther* **2021**, *6*, 425, doi:10.1038/s41392-021-00828-5.
49. Agilent (2014). CrysAlis PRO. Agilent Technologies Ltd, Yarnton, Oxfordshire, England.
50. Sheldrick, G.M. SHELXT – Integrated Space-Group and Crystal-Structure Determination. *Acta Cryst A* **2015**, *71*, 3–8, doi:10.1107/S2053273314026370.
51. Sheldrick, G.M. Crystal Structure Refinement with SHELXL. *Acta Cryst C* **2015**, *71*, 3–8, doi:10.1107/S2053229614024218.
52. Dolomanov, O.V.; Bourhis, L.J.; Gildea, R.J.; Howard, J. a. K.; Puschmann, H. OLEX2: A Complete Structure Solution, Refinement and Analysis Program. *J Appl Cryst* **2009**, *42*, 339–341, doi:10.1107/S0021889808042726.
53. Macrae, C.F.; Sovago, I.; Cottrell, S.J.; Galek, P.T.A.; McCabe, P.; Pidcock, E.; Platings, M.; Shields, G.P.; Stevens, J.S.; Towler, M.; et al. Mercury 4.0: From Visualization to Analysis, Design and Prediction. *J Appl Cryst* **2020**, *53*, 226–235, doi:10.1107/S1600576719014092.
54. Spek, A.L. Structure Validation in Chemical Crystallography. *Acta Cryst D* **2009**, *65*, 148–155, doi:10.1107/S090744490804362X.
55. Lee, C.; Yoon, J. UV Direct Photolysis of 2,2′-Azino-Bis(3-Ethylbenzothiazoline-6-Sulfonate) (ABTS) in Aqueous Solution: Kinetics and Mechanism. *Journal of Photochemistry and Photobiology A: Chemistry* **2008**, *197*, 232–238, doi:10.1016/j.jphotochem.2007.12.030.
56. Sharma, O.P.; Bhat, T.K. DPPH Antioxidant Assay Revisited. *Food Chemistry* **2009**, *113*, 1202–1205, doi:10.1016/j.foodchem.2008.08.008.
57. Maciejewska, K.; Czarnecka, K.; Kręcisz, P.; Niedziałek, D.; Wieczorek, G.; Skibiński, R.; Szymański, P. Novel Cyclopentaquinoline and Acridine Analogs as Multifunctional, Potent Drug Candidates in Alzheimer's Disease. *International Journal of Molecular Sciences* **2022**, *23*, 5876, doi:10.3390/ijms23115876.
58. Giske, C.G.; Turnidge, J.; Cantón, R.; Kahlmeter, G. Update from the European Committee on Antimicrobial Susceptibility Testing (EUCAST). *J Clin Microbiol 60*, e00276-21, doi:10.1128/jcm.00276-21.
59. Daina, A.; Michielin, O.; Zoete, V. SwissADME: A Free Web Tool to Evaluate Pharmacokinetics, Drug-Likeness and Medicinal Chemistry Friendliness of Small Molecules. *Sci Rep* **2017**, *7*, 42717, doi:10.1038/srep42717.
60. Daina, A.; Zoete, V. A BOILED-Egg To Predict Gastrointestinal Absorption and Brain Penetration of Small Molecules. *ChemMedChem* **2016**, *11*, 1117–1121, doi:10.1002/cmdc.201600182.

 doi:10.20944/preprints202604.0146.v1

61. Jones, G.; Willett, P.; Glen, R.C.; Leach, A.R.; Taylor, R. Development and Validation of a Genetic Algorithm for Flexible docking11Edited by F. E. Cohen. *Journal of Molecular Biology* **1997**, *267*, 727–748, doi:10.1006/jmbi.1996.0897.
62. Verdonk, M.L.; Cole, J.C.; Hartshorn, M.J.; Murray, C.W.; Taylor, R.D. Improved Protein–Ligand Docking Using GOLD. *Proteins: Structure, Function, and Bioinformatics* **2003**, *52*, 609–623, doi:10.1002/prot.10465.
63. Groom, C.R.; Bruno, I.J.; Lightfoot, M.P.; Ward, S.C. The Cambridge Structural Database. *Acta Cryst B* **2016**, *72*, 171–179, doi:10.1107/S2052520616003954.
64. Bollag, G.; Hirth, P.; Tsai, J.; Zhang, J.; Ibrahim, P.N.; Cho, H.; Spevak, W.; Zhang, C.; Zhang, Y.; Habets, G.; et al. Clinical Efficacy of a RAF Inhibitor Needs Broad Target Blockade in BRAF-Mutant Melanoma. *Nature* **2010**, *467*, 596–599, doi:10.1038/nature09454.
65. Pereira de Jésus-Tran, K.; Côté, P.-L.; Cantin, L.; Blanchet, J.; Labrie, F.; Breton, R. Comparison of crystal structures of human androgen receptor ligand-binding domain complexed with various agonists reveals molecular determinants responsible for binding affinity. *Protein Science* **2006**, *15*, 987–999, doi:10.1110/ps.051905906.
66. Stamos, J.; Sliwkowski, M.X.; Eigenbrot, C. Structure of the Epidermal Growth Factor Receptor Kinase Domain Alone and in Complex with a 4-Anilinoquinazoline Inhibitor*. *Journal of Biological Chemistry* **2002**, *277*, 46265–46272, doi:10.1074/jbc.M207135200.
67. Huet, J.; Teinkela Mbosso, E.J.; Soror, S.; Meyer, F.; Looze, Y.; Wintjens, R.; Wohlkönig, A. High-Resolution Structure of a Papaya Plant-Defence Barwin-like Protein Solved by in-House Sulfur-SAD Phasing. *Acta Cryst D* **2013**, *69*, 2017–2026, doi:10.1107/S0907444913018015.
68. Frisch, M.J.; Trucks, G.W.; Cheeseman, J.R.; Scalmani, G.; Caricato, M.; Hratchian, H.P.; Li, X.; Barone, V.; Bloino, J.; Zheng, G. Gaussian 09.
69. Laskowski, R.A.; Swindells, M.B. LigPlot+: Multiple Ligand–Protein Interaction Diagrams for Drug Discovery. *J. Chem. Inf. Model.* **2011**, *51*, 2778–2786, doi:10.1021/ci200227u.
70. Wallace, A.C.; Laskowski, R.A.; Thornton, J.M. LIGPLOT: A Program to Generate Schematic Diagrams of Protein-Ligand Interactions. *Protein Engineering, Design and Selection* **1995**, *8*, 127–134, doi:10.1093/protein/8.2.127.